J Ther Eng, Vol. 10, No. 2, pp. 286–298, March, 2024

Journal of Thermal Engineering
Web page info: https://jten.yildiz.edu.tr
DOI: 10.18186/thermal.1448571

Research Article

Performance evaluation of hybrid nanofluid-filled cylindrical heat pipe by machine learning algorithms

K. KUMARARAJA[1,*], B. SIVARAMAN[1], S. SARAVANAN[1]

[1]*Department of Mechanical Engineering, Annamalai University, Annamalainagar, Tamil Nadu, 608 002, India*

ARTICLE INFO

Article history
Received: 07 March 2023
Revised: 31 May 2023
Accepted: 01 June 2023

Keywords:
Cylindrical Heat Pipe; Error; Hybrid Nanofluid; Machine Learning; Outlet Temperature; Regression Algorithms

ABSTRACT

The current study attempts to predict the outlet temperature of a hybrid nanofluid heat pipe using three machine learning models, namely Extra Tree Regression (ETR), CatBoost Regression (CBR), and Light Gradient Boosting Machine Regression (LGBMR), in the Python environment. Based on 7000 experimental data (various heat input, inclination angle, flow rate, and fluid ratio), different training (95%–5%) and testing (5%–95%) split sizes, a closer prediction was attained at 85:15. The three attempted machine learning models are capable of predicting the outlet temperature, as evidenced by the less than 5% deviation from the experimental results. Of the three attempted machine learning models, the ETR model outperforms the other two with a higher accuracy (98%). Further, the sensitivity analysis indicates the absence of data overfitting in the attempted models.

Cite this article as: Kumararaja K, Sivaraman B, Saravanan S. Performance evaluation of hybrid nanofluid-filled cylindrical heat pipe by machine learning algorithms. J Ther Eng 2024;10(2):286–298.

INTRODUCTION

Heat pipes are one of the most efficient ways to transfer heat from one place to another. Heat pipes are a variety of heat exchangers frequently used in thermal energy recovery, energy conversion systems, solar collectors, spacecraft, and electronic and electrical equipment [1]. According to Chi [1], the use of heat pipes is the most efficient method to transfer heat between two interfaces. Meanwhile, Xu et al. [2] summarized the working fluids, operation mechanisms, and applications of heat pipes. In this juncture, Pathak et al. [3] and Dave et al. [4] in separate studies altered the working fluid, wick structure, and reported that the applied heat flux is the principal factor influencing the thermal performance of a heat pipe. On the contrary, Mehta et al. [5] altered geometric variables (channel size and shape), in a heat pipe, and concluded that the thermal resistance strongly depends on geometrical parameters. Likewise, Chernysheva et al. [6] analyzed the effect of external factors (device orientation, condenser cooling temperature, and condition of heat exchange with the surroundings), on the operating performance of a heat pipe. In a different attempt, Shafieian et al. [7] developed a theoretical model to determine the effect of operational variables on the thermal performance of heat pipe solar water heating systems. Similarly, Khan and Nadeem [8] developed a mathematical

***Corresponding author.**
*E-mail address: autpkkr@keemail.me

This paper was recommended for publication in revised form by Editor-in-Chief Ahmet Selim Dalkılıç

model to study the heat and mass transfer rates of the nanofluid in a stretching sheet. Likewise, Nadeem et al. successfully extended the mathematical model to a bio-convective micropolar nanofluid [9].

In the recent past, studies were conducted to investigate the effects of different working fluids and wick structure in a heat pipe, which are summarized here. Liang et al. employed neon as a working fluid and reported rapid acceleration of temperature to room temperature [10]. In a different attempt, a biporous wick was introduced by Zhang et al. and reported improved performance [11]. In a similar study, Zu et al. successfully performed a visualization study on boiling heat transfer in a heat pipe with a wire mesh wick [12]. However, recently, researchers focused their attention on nanofluids, which contain nanoparticles. Martin et al. [13] reported improved thermal efficiency while employing Fe-CuO hybrid nanofluid in heat pipes. In this context, Chabani et al. adjusted porous trapezoidal enclosure in a hybrid nanofluid and reported increased thermal efficiency [14]. In a different attempt, Mebarek-Oudina experimented with titania nanofluids in cylindrical annulus with a discrete heat source and opined that fluid properties impact the heat transfer rate [15]. In another study, the same research group employed the Buongiorno model to detect the thermal properties of the nanofluid [16]. In a different attempt, Pandya et al. [17] introduced an axial grooved heat pipe filled with CeO_2 + MWCNT/water-based nanofluid and reported that the particle concentration significantly influences the thermal performance of the heat pipe. Similarly, Bumataria et al. [18] evaluated the performance of a cylindrical heat pipe with water-based CuO and ZnO hybrid nanofluid and reported that the inclination affects the heat transfer rate significantly. Recently, Mebarek-Oudina and Chabani [19] wrote a review on the applications and heat transfer enhancement techniques employing nanofluids at different enclosures. Dharmaiah et al. [20] developed a mathematical model to analyze the heat transfer rate in a nuclear reactor. Meanwhile, a group of researchers from Pakistan, determined the performance of heat pipe with different nanofluids through a theoretical approach [21–25].

Despite the effectiveness of the experimental approach, its complexity and time-consuming nature encourage researchers to seek a quick and dependable solution. In recent years, there has been a rise in the use of software for predicting the thermal performance of a heat pipe. The more recent technology, machine learning, aids in the identification of potentially challenging correlations that may exist within the dataset, enabling us to acquire a better depiction of the process. Ahmad et al. [26] recommended the ETR model while predicting solar thermal energy efficiency. Meanwhile, Xiang et al. [27] attempted a CBR model for predicting power load and reported less error variance. In a different attempt, Gong et al. [28] predicted the return temperature of district heating systems and recommended the LGBMR model for better prediction.

Based on the review of the literature, though studies on the usage of nanofluids in heat pipes have been attempted, the application of machine learning techniques to predict the performance of hybrid nanofluid heat pipes is scarce. In particular, the prediction of the outlet temperature in the heat pipe utilizing hybrid nanofluid has not yet been implemented using machine learning techniques like Extra Tree Regression (ETR), CatBoost Regression (CBR), and Light Gradient Boosting Machine Regression (LGBMR). Hence, ETR, CBR, and LGBMR models are employed to predict the outlet temperature of the heat pipe with hybrid nanofluid, and the deviation from the experimental results is reported.

MATERIALS AND METHODS

Preparation of Hybrid Nanofluids

The silver nanoparticles were synthesized using a one-step chemical reduction technique. Using the Lee-Meisel process, silver nitrate is reduced with trisodium citrate in double-distilled water at a volume concentration of 0.01% to yield silver nanofluid [29]. Alumina nanofluid was produced by a two-step ultrasonication process. a) Heating an aqueous solution of aluminum nitrate and b) urea to the appropriate concentration produced an alumina nanoparticle [30]. By using ultrasonication, synthetic alumina nanoparticles were combined with double-distilled water at a volume concentration of 0.01% to produce alumina nanofluid. The traditional tests of UV absorption (Figure 1) and size distribution (Figure 2) analysis were used to confirm the presence of silver and alumina nanofluids. The hybrid nanofluid charge in the heat pipe was 16 ml [1], and the fill percentage was 37.62%. Three Ag-Al_2O_3 ratios of 80%–20%, 70%–30%, and 60%–40% hybrid nanofluids were created, as detailed in Table 1, to study the thermal performance of heat pipe.

Table 1. Compositions of hybrid nanofluid

Working fluid	Ag/ distilled water (ml)	Al_2O_3/ distilled water (ml)	Total hybrid nanofluid (ml)
(Ag 80%-Al_2O_3 20%)/ distilled water	12.8	3.2	16
(Ag 70%-Al_2O_3 30%)/ distilled water	11.2	4.8	16
(Ag 60%-Al_2O_3 40%)/ distilled water	9.6	6.4	16

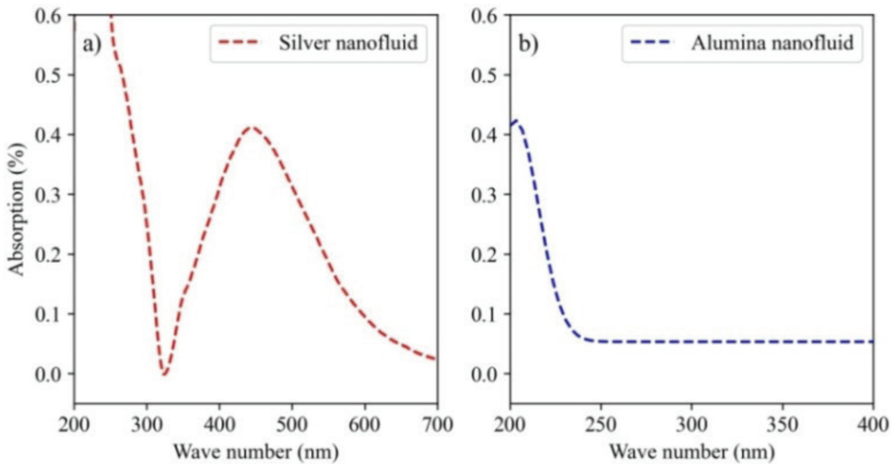

Figure 1. UV absorption characteristic test of **a)** silver nanofluid and **b)** alumina nanofluid.

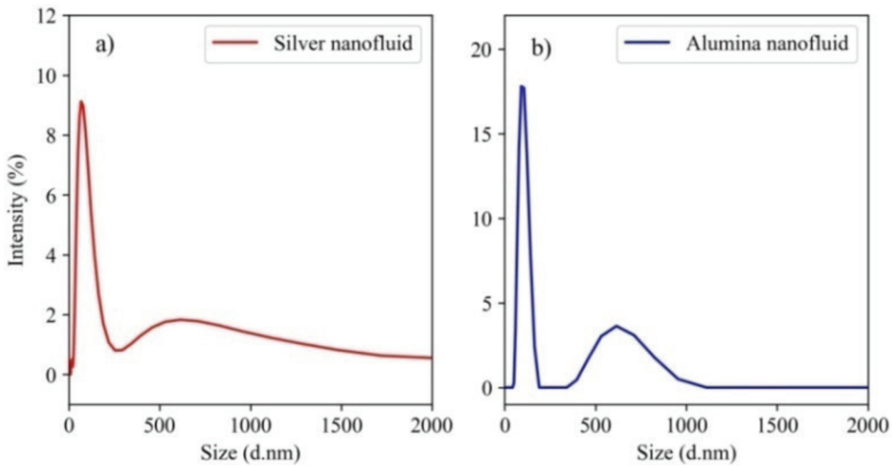

Figure 2. Size distribution analysis of **a)** silver nanofluid and **b)** alumina nanofluid.

Experimental Setup

The heat pipe was designed using the procedure given by Chi [1], and the heat pipe's capillary heat transport, sonic, entrainment, and boiling limitations were calculated. The calculated capillary heat transport limitation was 100 W. Consequently, the heat input was limited to 100 W. The heat pipe was made of copper. The wick inside the heat pipe is made of stainless steel screen mesh. The inner surface of the heat pipe was rolled with two layers of stainless steel screen mesh. Copper end caps were used to perfectly seal the ends of the heat pipe. To create vacuum inside the heat pipe, a vacuum pump and a vacuum pressure gauge were utilized. The specifications of the heat pipe are shown in Table 2. The schematic diagram of the heat pipe with vacuum gauge is shown in Figure 3. Three hybrid nanofluid ratios were sequentially charged with 16 ml each inside the heat pipe's cylindrical heat pipe. First, 80%–20% hybrid nanofluid was charged into the heat pipe. Secondly, the test has been carried out. Thirdly, by completing the experiment, the hybrid nanofluid of 80%–20% has been fully drained, and the remaining experiments were conducted with 70%–30% and 60%–40% hybrid nanofluids. A 500 W heater (Venus: copper coil with ceramic insulator) was positioned circumferentially at the outer edge of the heat pipe in the evaporator section.

The power supply for the heater is at 240 volts and 50 Hz. A voltage regulator (Cresta autostat) was used to regulate the power supply, and a digital wattmeter (Cabs electra) was used to measure the amount of heat input. Black rubber foam was used as insulation in the adiabatic portion to reduce heat loss from the heat pipe. A cylindrical shell with a diameter of 35 mm was constructed for the condenser section, and water circulated naturally within it to serve as a coolant. The cylindrical heat pipe and the atmospheric temperature were measured and monitored using nine T-type thermocouples (T1 – T9), as shown in Figure 3. The temperature data was measured, tracked, and collected every 30 s using an Agilent data logger (Model No. 34970A) with a desktop computer. The camera-friendly view and the schematic diagram of the experimental setup are shown in Figs. 4a and 4b, respectively. The heat input was varied from 40 W to 100 W (in steps of 10 W), and the inclination was varied by 0°, 30°, and 45°. The flow rate was varied by 0.0033 kg/s and 0.0050 kg/s, and the fluid ratio was fixed at 0.6 (60%–40%), 0.7 (70%–30%), and 0.8 (80%–20%), respectively. These parameters were fixed by trial and error. The minimum and maximum values of each process parameter are displayed in Table 3.

MACHINE LEARNING ALGORITHMS

Extra Tree Regression (ETR)

Extra tree, also known as much randomized trees, is an ensemble-supervised machine learning technique that trains models using the decision tree algorithm. The decision trees function with classification and regression techniques. This approach is comparable to random forests but may be faster. Similar to the random forest technique, the additional trees algorithm generates numerous decision trees, but the sampling for each tree is random and without replacement. As a result, each tree gets its own dataset with distinct samples. Additionally, each tree receives a random selection of a predetermined number of features from the entire set of features. The choice of a feature's splitting value is made at random, which is the most significant and

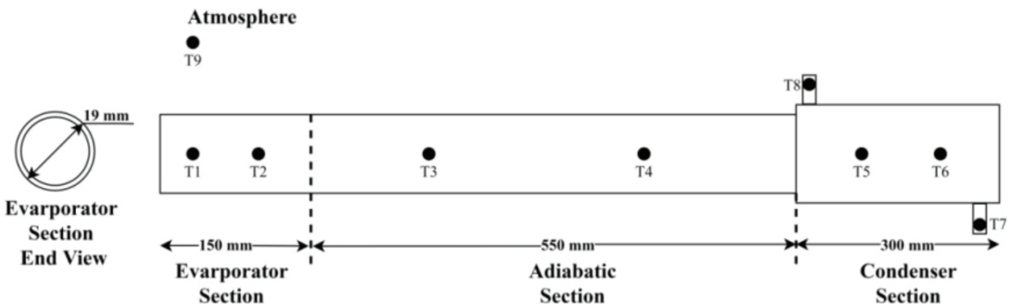

Figure 3. Schematic diagram of the heat pipe.

(1: Heat pipe, 2: Inclination arrangement, 3: Water line, 4: Main power supply, 5: Voltage regulators, 6: Watt meters, 7: T – type thermocouples, 8: Agilent data logger, 9: Desktop computer, and 10: Vacuum pressure gauge)

Figure 4a. Photographic view of the experimental setup.

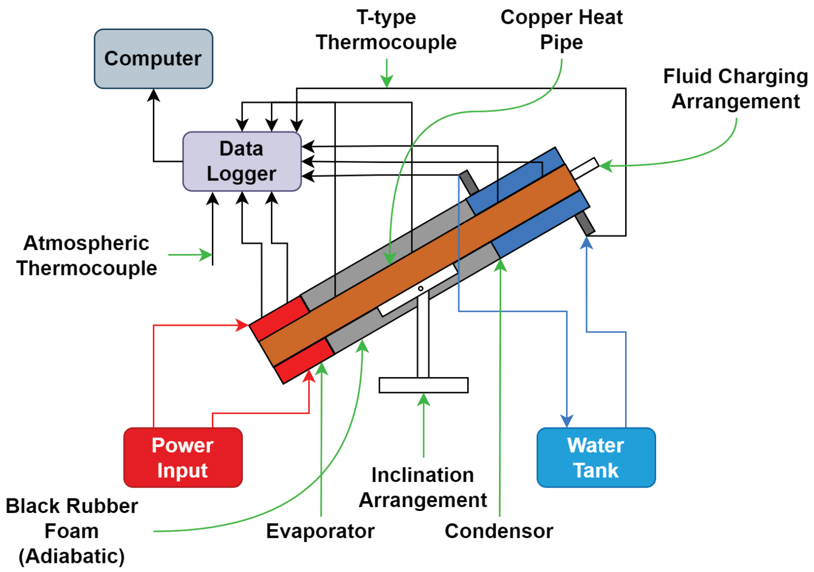

Figure 4b. Schematic diagram of the experimental setup.

Table 2. Specifications of the heat pipe

Specifications	Dimensions
Total length (mm)	1000
Inner diameter (mm)	17
Outer diameter (mm)	19
Thickness (mm)	2
Evaporator section (mm)	150
Adiabatic section (mm)	550
Condenser section (mm)	300
Condenser diameter (mm)	35
Mesh size	20,000 per mm^2
Heating coil length (mm)	150
Pipe material	Copper
Wick material	Stainless steel
Wick structure	Wrapped screen (Two layers)
Fill ratio (%)	37.62

Table 3. Range of the parameters

Parameters	Range (Raw data)	
	Min	Max
Heat input (W)	40	100
Inclination (°)	0	45
Flow rate (kg/ s)	0.0033	0.0050
Fluid ratio (Ag-Al_2O_3)	0.6 (60%-40%)	0.8 (80%-20%)
Condenser inlet temperature (K)	302.68	309.25
Atmospheric temperature (K)	301.27	308.00
Outlet temperature (K)	303.60	320.73

distinctive property of additional trees. The approach randomly chooses a split value for the data instead of finding a locally optimal value using gini or entropy. As a result, the trees are diverse and uncorrelated [31].

Catboost Regression (CBR)

CatBoost is a supervised machine learning technique that solves classification and regression issues by using decision trees. As the name implies, CatBoost has two key components: gradient boosting (the Boost) and categorical data (the Cat) to work with data. Gradient boosting is a method where several decision trees are built iteratively. Each additional tree enhances the output of the previous one, producing greater outcomes. For faster implementation, CatBoost enhances the initial gradient boost technique. CatBoost bypasses a drawback of conventional decision tree-based approaches, where the data must often be pre-processed to transform categorical string variables to numerical values, one-hot encodings, etc. This approach can use a mix of category and non-categorical explanatory variables directly, without any preprocessing. In this algorithm, preprocessing is included. The categorical features in CatBoost are encoded using a technique known as ordered encoding. When using ordered encoding, a value is generated to replace the categorical feature that takes into account the target statistics from all the rows prior to a data point. CatBoost uses symmetric trees, which is another distinctive feature of it. As a result, every decision node at every depth level employs the identical split condition [32].

Light Gradient Boosting Machine Regression (LGBMR)

The Light Gradient Boosting Machine is a gradient-boosting ensemble technique used to train decision trees. Both classification and regression problems can be solved with LGBMR. LGBMR is designed for high performance in distributed systems. When using LGBMR to generate decision trees, just one leaf is split for each condition, depending on the gain, and the trees develop in a leaf wise manner. Sometimes, especially with smaller datasets, leaf-wise trees might overfit. Overfitting can be prevented by restricting the tree depth. A histogram of the distribution is used by LGBMR to bucket data into bins. For iteration, gain calculation, and data splitting, the bins are employed rather than each data point. Additionally, a sparse dataset can benefit from this method's optimization. Another element of LGBMR is exclusive feature bundling, in which the algorithm bundles exclusive characteristics to reduce dimensionality and make it quicker and more efficient [33].

Methodologies Adopted to Select the Training and Testing Sizes

In this study, the outlet temperature of a cylindrical screen-mesh heat pipe filled with hybrid nanofluid was analyzed and estimated using ETR, CBR, and LGBMR regression models. Heat inputs, inclinations, flow rates, fluid ratios, condenser inlet temperature, and ambient temperature were chosen as input parameters. The output temperature is the target parameter. To determine the best split size, the dataset is divided into different training and testing sizes, ranging from 95%: 5% to 5%: 95% in steps of -5%: +5% for all these regression models. R^2 was used to determine the accuracy of every split size (Table 4).

Hyperparameters Tuning of ETR, CBR and LGBMR Models

Each model has a collection of hyperparameters that affect its accuracy, robustness, and capacity to learn from new datasets. The hyperparameters significantly influence the computation time as well. Tuning the hyperparameters is necessary in order to maximize the model's performance. In this study, the models of ETR, CBR, and LGBMR, are tuned to achieve the best accuracy. It is carried out using the Optuna (a Bayesian optimizer) framework, which uses the R^2 value as an accuracy benchmark to determine which model parameters are the best to tweak. The tuned hyperparameters for the models ETR, CBR, and LGBMR are shown in Table 5. Three performance indicators, namely mean absolute error (MAE), mean absolute percentage error (MAPE), and R^2 value, were used to assess the outlet temperature prediction accuracy. These metrics are employed to assess the variance between the outlet temperature that results from the experimental approach and the predicted outlet temperature. The performance indicators are computed as follows:

Table 4. Training and testing combinations (optimal condition highlighted)

Training and testing combination (%:%)	Models		
	CBR	ETR	LGBMR
95:5	0.9856	0.9869	0.9726
90:10	0.9857	0.9870	0.9727
85:15	**0.9859**	**0.9871**	**0.9728**
80:20	0.9850	0.9865	0.9719
75:25	0.9849	0.9859	0.9714
70:30	0.9849	0.9861	0.9715
65:35	0.9841	0.9850	0.9712
60:40	0.9839	0.9846	0.9711
55:45	0.9831	0.9844	0.9706
50:50	0.9832	0.9840	0.9698
45:55	0.9822	0.9836	0.9683
40:60	0.9817	0.9825	0.9679
35:65	0.9815	0.9826	0.9675
30:70	0.9797	0.9817	0.9656
25:75	0.9788	0.9803	0.9645
20:80	0.9773	0.9779	0.9596
15:85	0.9742	0.9723	0.9546
10:90	0.9652	0.9632	0.9535
5:95	0.9471	0.9400	0.9384

$$MAE = \frac{\sum_{i=1}^{n}\left|y_e - y_p\right|}{n} \quad (1)$$

$$MAPE = \frac{\sum_{i=1}^{n}\left|\frac{y_e - y_p}{y_e}\right|}{n} \quad (2)$$

$$R^2 = 1 - \left(\frac{\sum_{i=1}^{n}\left(y_e - y_p\right)^2}{\sum_{i=1}^{n}\left(y_e - y_{e,mean}\right)^2}\right) \quad (3)$$

RESULTS AND DISCUSSION

Experimental Results

The experimental condition (Q: 100W, I: 45°, ṁ: 0.0050 kg/s, and R: 0.8) produced the highest outlet temperature of 320.726 K, whereas the operating state (Q: 40W, I: 0°, ṁ: 0.0033 kg/s, and R: 0.6) resulted in the lowest outlet temperature (303.6 K). The maximum outlet temperature is produced when the working fluid has the highest silver content (80%), consistent with the reports of Chavda and Bumataria [34]. Increases in the heat input, inclination, flow rate, and silver content resulted in a higher outlet temperature compatible with the studies carried out by Ali et al. [35]. The operating parameters (Q, I, ṁ and R) significantly affect the outlet temperature.

Prediction of Outlet Temperature by the Developed Models: A Comparative Analysis

The accuracy of the models is revealed by a scatter plot (Figure 5 a–c) between the actual and predicted output temperatures. According to experimental results, all the machine learning models attempted displayed significant or foggy dispersion around the diagonal. The fogginess suggests a close correlation between the experimental and predicted values. The closer distance between the predicted values and the diagonal line is a sign of higher accuracy. Yang et al. [36] opined that the model performs well if the scatter points are close to the diagonal line; but poorly if the scatter points are distant from the diagonal line. The scatter distributions of the ETR and CBR models are more tightly packed towards the centre diagonal line compared to the LGBMR model. In terms of scatter distribution, the ETR model outperforms all others with the least amount of deviation from the diagonal, consistent with the studies carried out by Khan and Nadeem [37]. The performance and accuracy metrics for each of the three machine learning models are tabulated in Table 6.

The MAE and MAPE values in the LGBMR model are higher (Table 6), which results in lower R^2 values. In terms of accuracy, the ETR model outperforms the other two machine learning models since it has lower MAE and MAPE values (0.0955 and 0.0310) and a higher R^2 value (0.9890), which is consistent with the separate studies of Khan et al. [38] and Nadeem et al. [39]. As a result, the Extra Tree Regression model is recommended for predicting the outlet temperature of the heat pipe when employing hybrid nanofluid.

Table 5. Tuned hyperparameters.

Model	Hyperparameters	Range	Optimal value
ETR	max_depth	2-1000	615
	max_leaf_nodes	2-1000	542
	min_samples_split	2-1000	2
	n_estimators	2-1000	808
CBR	l2_leaf_reg	$1e^{-3}$-10	0.04
	learning_rate	0.006-0.018	0.006
	max_bin	200-400	215
	max_depth	5-15	13
	min_data_in_leaf	1-300	52
	subsample	0.4-1	0.6
LGBMR	lambda_l1	$1e^{-5}$-$1e^{-1}$	0.01
	learning_rate	$1e^{-3}$-10	0.33
	max_bin	80-300	137
	min_data_in_leaf	10-80	35
	min_sum_hessian_in_leaf	$1e^{-8}$-10	$7.46e^{-7}$
	num_leaves	10-30	11
	path_smooth	0.4-1.5	0.43
	verbose	1-5	4

Table 6. Performance metrics of the models.

Model	Metrics	Dataset			
		Total	Train	Test	Validation
	MAE	**0.0692**	**0.0636**	**0.0955**	**0.1333**
ETR	**MAPE**	**0.0225**	**0.0206**	**0.0310**	**0.0433**
	R^2	**0.9945**	**0.9957**	**0.9890**	**0.9804**
	MAE	0.0917	0.0902	0.0993	0.1339
CBR	MAPE	0.0298	0.0293	0.0322	0.0437
	R^2	0.9903	0.9908	0.9882	0.9790
	MAE	0.1131	0.1110	0.1542	0.1440
LGBMR	MAPE	0.0367	0.0360	0.0500	0.0467
	R^2	0.9858	0.9863	0.9731	0.9725

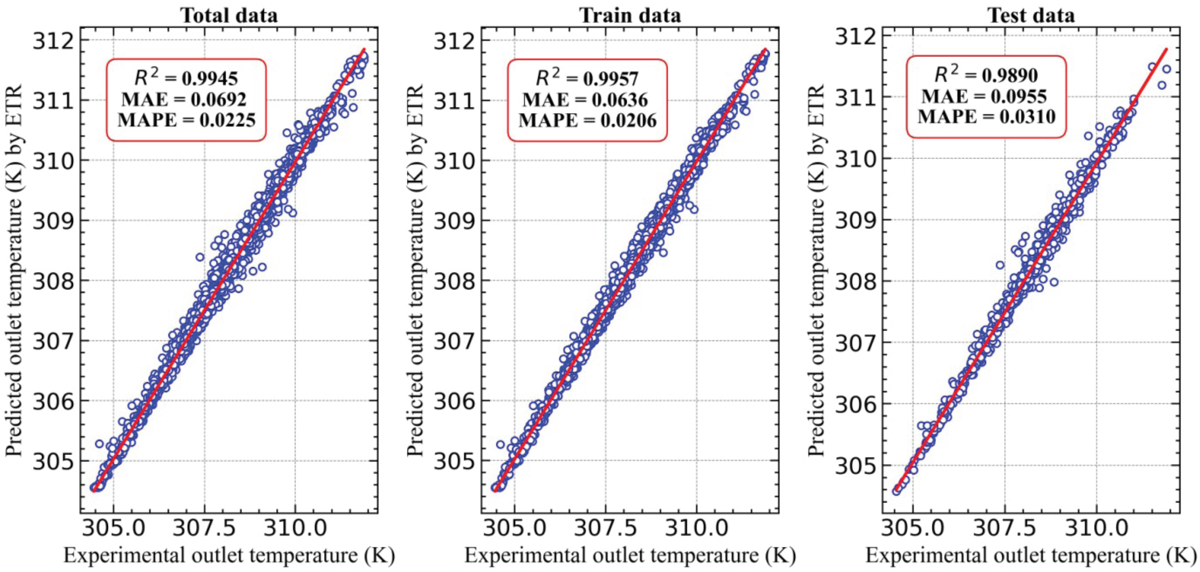

Figure 5a. Regression plots for ETR model.

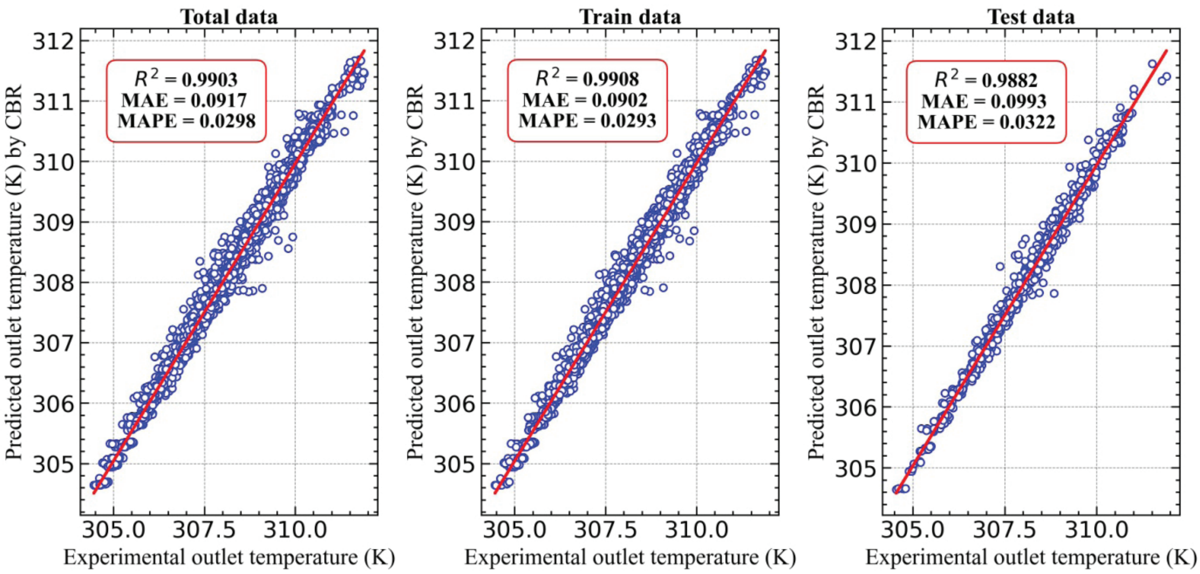

Figure 5b. Regression plots for CBR model.

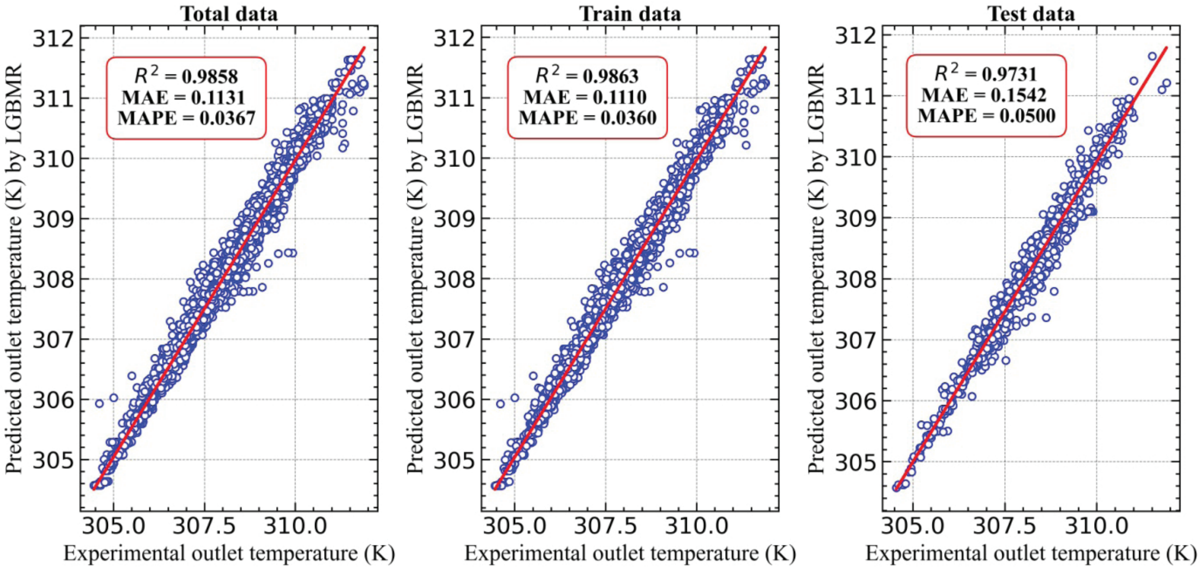

Figure 5c. Regression plots for LGBMR model.

Sensitivity Analysis

To cross-validate the attempted models and ensure their accuracy, a sensitivity analysis was carried out. With 15 data points, Table 7 shows the outflow temperature under the experimental conditions. The proposed machine learning models (ETR, CBR, and LGBMR) are also shown together with the predicted values under the aforementioned conditions. The validation data for the model's accuracy are shown in a scatter plot (Figure 6 a–c) between the actual and predicted outlet temperatures. The scatter distributions of the ETR and CBR models are more tightly packed towards the centre diagonal line compared to the LGBMR model. Table 7 presents the difference in error between experimental and predicted findings, while Table 6 displays, correspondingly, their performance metrics. The R^2 values of the sensitivity analysis data and test data are 0.67% and 1.54% different from the training data, respectively, indicating the variance is not substantial. According to Shafiq et al. [40] and Singh and Gupta [41], if the deviation is less than 5%, the models are suitable for prediction, which is in agreement with the present study. It is concluded that the models are capable of producing reasonable predictions without experiencing significant overfitting. The optimal parametric conditions determined by the ETR model to attain maximum outlet temperature are Q-98.54 W, I-43.49°, $\dot{m}$-0.0044 kg/s and R-0.77.

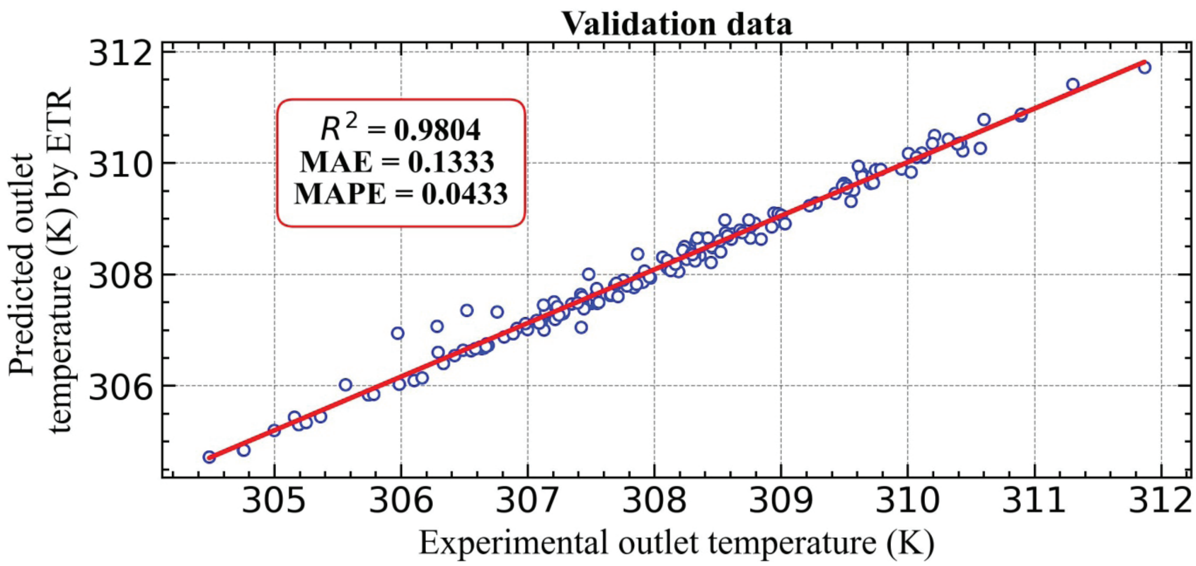

Figure 6a. Regression plots for ETR model (validation).

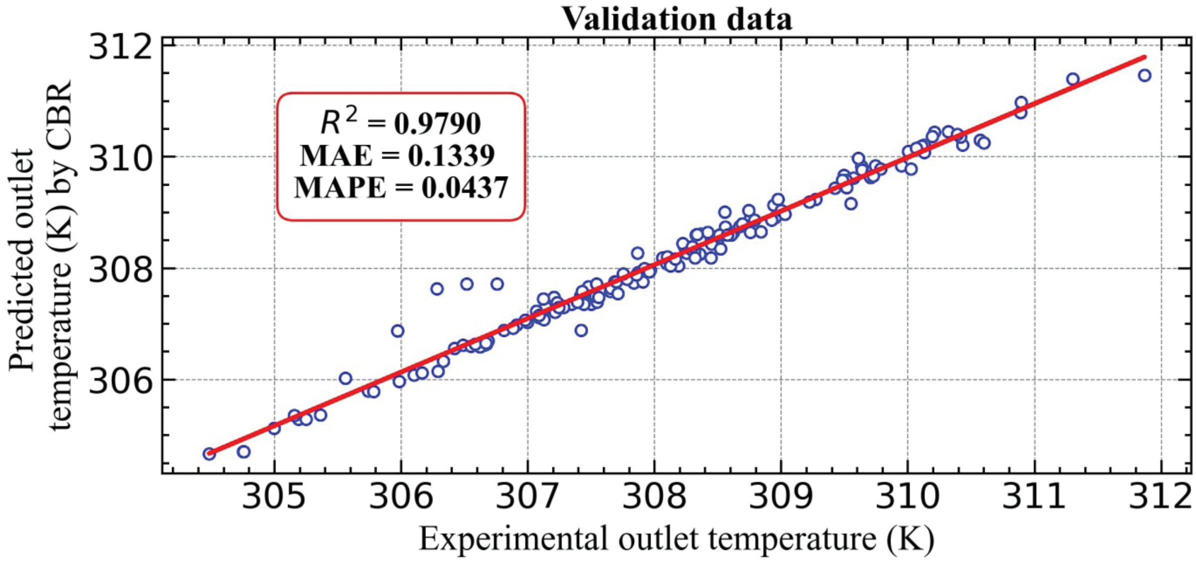

Figure 6b. Regression plots for CBR model (validation).

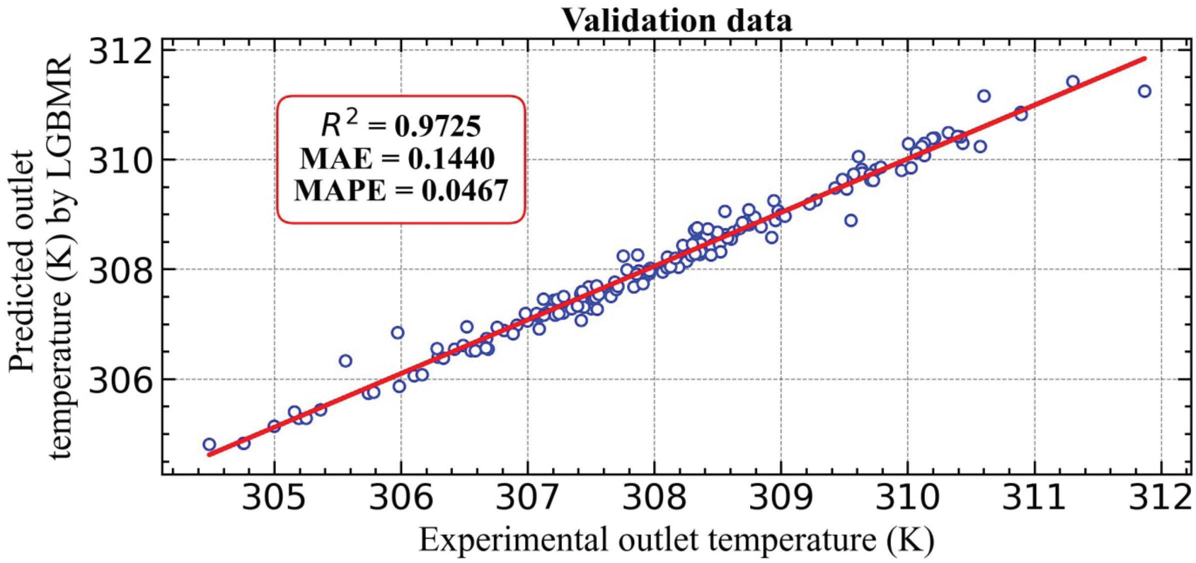

Figure 6c. Regression plots for LGBMR model (validation).

CONCLUSION AND FUTURE RECOMMENDATIONS

- The optimal training and testing split sizes were 85% and 15%, respectively.
- With a deviation of less than 5%, attempted machine learning models effectively predict the output temperature.
- The ETR model was the most accurate, followed by the CBR and LGBMR models due to its ensemble learning algorithm and randomized selection of split values.
- It is recommended to employ a 0.77 fluid ratio with a heat input of Q = 98.54 W, an inclination of I = 43.49°, and a flow rate of $\dot{m}$ = 0.0044 kg/s to attain higher outlet temperature.
- The sensitivity analysis showed that the attempted machine learning models did not exhibit data overfitting.

This study shows that the ETR, CBR, and LGBMR machine learning regression models have good potential for predicting the outlet temperature of a cylindrical screen-mesh heat pipe filled with hybrid nanofluid. However, additional research needs to be done with more experimental data on various geometrical, fluid properties, operational, and ambiance variables to find a responsible design tool for the use of hybrid nanofluids in heat pipes.

Table 7. Error differences among the models.

Exp. No.	Q (W)	I (o)	$\dot{m}$ (kg/s)	R	Ti (K)	Ta (K)	To (K) Exp. (K)	Predicted ETR	Predicted CBR	Predicted LGBMR	Error (K) ETR	Error (K) CBR	Error (K) LGBMR
1	100	0	0.0033	0.6	306.166	306.743	311.299	311.1673	311.4969	311.3897	0.1317	-0.1979	-0.0907
2	70	30	0.0033	0.6	305.082	304.276	308.235	308.0489	308.3760	307.3438	0.1861	-0.1410	0.8912
3	40	30	0.0033	0.6	305.701	304.126	307.086	307.0938	307.3620	306.9828	-0.0078	-0.2760	0.1032
4	80	30	0.0033	0.6	306.413	306.426	309.949	309.7319	309.8757	310.2944	0.2171	0.0733	-0.3454
5	70	30	0.005	0.6	305.136	305.262	307.139	307.2407	307.2541	307.2430	-0.1017	-0.1151	-0.1040
6	70	45	0.005	0.7	305.532	304.066	307.207	307.4195	307.5238	307.2505	-0.2125	-0.3168	-0.0435
7	80	30	0.0033	0.7	307.129	305.009	310.432	309.8402	310.0689	309.2999	0.5918	0.3631	1.1321
8	100	30	0.005	0.7	305.693	305.004	308.557	308.4822	308.5933	307.2975	0.0748	-0.0363	1.2595
9	40	45	0.005	0.8	303.651	302.453	304.752	304.6577	304.6581	304.6567	0.0943	0.0939	0.0953
10	70	45	0.005	0.6	306.262	306.052	308.329	308.4966	308.5376	308.3559	-0.1676	-0.2086	-0.0269
11	100	45	0.0033	0.6	306.417	305.883	311.869	311.0391	311.0606	311.2994	0.8299	0.8084	0.5696
12	50	30	0.0033	0.8	305.723	303.430	307.652	307.1697	307.5975	307.5059	0.4823	0.0545	0.1461
13	60	30	0.0033	0.8	304.396	303.401	306.912	306.7549	306.9852	306.9221	0.1571	-0.0732	-0.0101
14	70	30	0.005	0.6	305.183	304.809	307.175	307.2418	307.4062	306.9168	-0.0668	-0.2312	0.2582
15	80	45	0.0033	0.7	305.909	305.269	308.940	309.1136	309.1979	309.2761	-0.1736	-0.2579	-0.3361

NOMENCLATURE

Abbreviations

$\dot{m}$	Flow rate (kg/s)
CBR	CatBoost Regression
ETR	Extra Tree Regression
Exp.	Experiments
I	Inclination (°)
i	Index number
IDE	Integrated Development Environment
LGBMR	Light Gradient Boosting Machine Regression
MAE	Mean Absolute Error
MAPE	Mean Absolute Percentage Error
MWCNT	Multi-Walled Carbon NanoTubes
n	Number of data points
Q	Heat input (W)
R	Fluid ratio
R^2	Determination of Coefficient
T_a	Atmospheric temperature (K)
T_i	Condenser inlet temperature (K)
T_o	Outlet temperature (K)
y_e	Actual value
$y_{e,mean}$	Actual mean value
Y_p	Predicted value

Chemical symbols

CeO_2	Cerium oxide
CuO	Copper oxide
Fe	Iron
ZnO	Zinc oxide

ACKNOWLEDGEMENT

The authors wish to express their sincere thanks to the authorities of Annamalai University for permitting to utilize the facilities to carry out this research work.

DISCLOSURE STATEMENT

The authors declare no conflict of interest.

AUTHORSHIP CONTRIBUTIONS

Authors equally contributed to this work.

DATA AVAILABILITY STATEMENT

The authors confirm that the data that supports the findings of this study are available within the article. Raw data that support the finding of this study are available from the corresponding author, upon reasonable request.

CONFLICT OF INTEREST

The author declared no potential conflicts of interest with respect to the research, authorship, and/or publication of this article.

ETHICS

There are no ethical issues with the publication of this manuscript.

REFERENCES

[1] Chi SW. Heat Pipe Theory and Practice: A Sourcebook. New York: McGraw-Hill; 1976.

[2] Xu Y, Xue Y, Qi H, Cai W. An updated review on working fluids, operation mechanisms, and applications of pulsating heat pipes. Renew Sust Energy Rev 2021;144:110995. [CrossRef]

[3] Pathak SK, Kumar R, Goel V, Pandey AK, Tyagi VV. Recent advancements in thermal performance of nano-fluids charged heat pipes used for thermal management applications: A comprehensive review. Appl Therm Eng 2022;216:119023. [CrossRef]

[4] Dave C, Dandale P, Shrivastava K, Dhaygude D, Rahangdale K, More N. A review on pulsating heat pipes: latest research, applications and future scope. J Therm Eng 2021;7:387–408. [CrossRef]

[5] Mehta K, Mehta N, Patel V. Experimental investigation of the thermal performance of closed loop flat plate oscillating heat pipe. Exp Heat Transf 2021;34:85–103. [CrossRef]

[6] Chernysheva MA, Yushakova SI, Maydanik YF. Effect of external factors on the operating characteristics of a copper-water loop heat pipe. Int J Heat Mass Transf 2015;81:297–304. [CrossRef]

[7] Shafieian A, Khiadani M, Nosrati A. Thermal performance of an evacuated tube heat pipe solar water heating system in cold season. Appl Therm Eng 2019;149:644–657. [CrossRef]

[8] Khan MN, Nadeem S. Theoretical treatment of bio-convective Maxwell nanofluid over an exponentially stretching sheet. Can J Phys 2020;98:732–741. [CrossRef]

[9] Nadeem S, Khan MN, Muhammad N, Ahmad S. Mathematical analysis of bio-convective micropolar nanofluid. J Comput Des Eng 2019;6:233–242. [CrossRef]

[10] Liang Q, Li Y, Wang Q. Experimental investigation on the performance of a neon cryogenic oscillating heat pipe. Cryogenics 2017;84:7–12. [CrossRef]

[11] Zhang Z, Zhao R, Liu Z, Liu W. Application of biporous wick in flat-plate loop heat pipe with long heat transfer distance. Appl Therm Eng 2021;184:116283. [CrossRef]

[12] Zu S, Liao X, Huang Z, Li D, Jian Q. Visualization study on boiling heat transfer of ultra-thin flat heat pipe with single layer wire mesh wick. Int J Heat Mass Transf 2021;173:121239. [CrossRef]

[13] Martin K, Sözen A, Çiftçi E, Ali HM. An experimental investigation on aqueous Fe-CuO hybrid nanofluid usage in a plain heat pipe. Int J Thermophys 2020;41:135. [CrossRef]

[14] Chabani I, Mebarek-Oudina F, Vaidya H, Ismail AI. Numerical analysis of magnetic hybrid nanofluid natural convective flow in an adjusted porous trapezoidal enclosure. J Magn Magn Mater 2022;564:170142. [CrossRef]

[15] Mebarek-Oudina F. Convective heat transfer of Titania nanofluids of different base fluids in cylindrical annulus with discrete heat source. Heat Transf-Asian Res 2019;48:135–147. [CrossRef]

[16] Mebarek-Oudina F, Preeti, Sabu AS, Vaidya H, Lewis RW, Areekara S, et al. Hydromagnetic flow of magnetite-water nanofluid utilizing adapted Buongiorno model. Int J Mod Phys B 2023:2450003. [CrossRef]

[17] Pandya NS, Desai AN, Kumar Tiwari A, Said Z. Influence of the geometrical parameters and particle concentration levels of hybrid nanofluid on the thermal performance of axial grooved heat pipe. Therm Sci Eng Prog 2021;21:100762. [CrossRef]

[18] Bumataria RK, Chavda NK, Nalbandh AH. Performance evaluation of the cylindrical shaped heat pipe utilizing water-based CuO and ZnO hybrid nanofluids. Energy Source Part A 2020;0:1–16. [CrossRef]

[19] Mebarek-Oudina F, Chabani I. Review on nano-fluids applications and heat transfer enhancement techniques in different enclosures. J Nanofluids 2022;11:155–168. [CrossRef]

[20] Dharmaiah G, Mebarek-Oudina F, Sreenivasa Kumar M, Chandra Kala K. Nuclear reactor application on Jeffrey fluid flow with Falkner-skan factor, Brownian and thermophoresis, non linear thermal radiation impacts past a wedge. J Indian Chem Soc 2023;100:100907. [CrossRef]

[21] Khan MN, Nadeem S, Muhammad N. Micropolar fluid flow with temperature-dependent transport properties. Heat Transf 2020;49:2375–2389. [CrossRef]

[22] Ahmad S, Nadeem S, Muhammad N, Khan MN. Cattaneo-Christov heat flux model for stagnation point flow of micropolar nanofluid toward a nonlinear stretching surface with slip effects. J Therm Anal Calorim 2021;143:1187–1199. [CrossRef]

[23] Ahmad S, Khan MN, Nadeem S. Mathematical analysis of heat and mass transfer in a Maxwell fluid with double stratification. Phys Scr 2020;96:025202. [CrossRef]

[24] Khan MN, Ullah N, Nadeem S. Transient flow of Maxwell nanofluid over a shrinking surface: numerical solutions and stability analysis. Surf Interface 2021;22:100829. [CrossRef]

[25] Khan MN, Nadeem S, Ullah N, Saleem A. Theoretical treatment of radiative Oldroyd-B nanofluid with microorganism pass an exponentially stretching sheet. Surf Interface 2020;21:100686. [CrossRef]

[26] Ahmad MW, Reynolds J, Rezgui Y. Predictive modelling for solar thermal energy systems: A comparison of support vector regression, random forest, extra trees and regression trees. J Clean Prod 2018;203:810–821. [CrossRef]

[27] Xiang W, Xu P, Fang J, Zhao Q, Gu Z, Zhang Q. Multi-dimensional data-based medium- and long-term power-load forecasting using double-layer CatBoost. Energy Rep 2022;8:8511–22. [CrossRef]

[28] Gong M, Bai Y, Qin J, Wang J, Yang P, Wang S. Gradient boosting machine for predicting return temperature of district heating system: A case study for residential buildings in Tianjin. J Build Eng 2020;27:100950. [CrossRef]
[29] Dong B, Xue N, Mu G, Wang M, Xiao Z, Dai L, et al. Synthesis of monodisperse spherical AgNPs by ultrasound-intensified Lee-Meisel method, and quick evaluation via machine learning. Ultrason Sonochem 2021;73:105485. [CrossRef]
[30] Sakthivadivel D, Ganesh Kumar P, Prabakaran R, Vigneswaran VS, Nithyanandhan K, Kim SC. A neem oil-based biodiesel with DEE enriched ethanol and Al_2O_3 nano additive: An experimental investigation on the diesel engine performance. Case Stud Therm Eng 2022;34:102021. [CrossRef]
[31] Heddam S, Ptak M, Zhu S. Modelling of daily lake surface water temperature from air temperature: Extremely randomized trees (ERT) versus Air2Water, MARS, M5Tree, RF and MLPNN. J Hydrol 2020;588:125130. [CrossRef]
[32] Abdurakipov SS, Kiryukhina NV, Butakov EB. Prediction of boiling crisis in channels using machine learning algorithms. Optoelect Instrument Data Process 2022;58:98−108. [CrossRef]
[33] Chun P, Izumi S, Yamane T. Automatic detection method of cracks from concrete surface imagery using two-step light gradient boosting machine. Comput-Aided Civ Inf 2021;36:61−72. [CrossRef]
[34] Chavda N, Bumataria R. Effect of particle size and concentration on thermal performance of cylindrical shaped heat pipe using silver-DI water nanofluid. Int J Ambient Energy 2023;44:305−316. [CrossRef]
[35] Ali B, Qayoum A, Saleem S, Mir FQ. Experimental investigation of nanofluids for heat pipes used in solar photovoltaic panels. J Therm Eng 2023:439−456. [CrossRef]
[36] Yang W, Shen P, Ye Z, Zhu Z, Xu C, Liu Y, et al. Adversarial training collaborating multi-path context feature aggregation network for maize disease density prediction. Processes 2023;11:1132. [CrossRef]
[37] Khan MN, Nadeem S. A comparative study between linear and exponential stretching sheet with double stratification of a rotating Maxwell nanofluid flow. Surf Interface 2021;22:100886. [CrossRef]
[38] Khan U, Mebarek-Oudina F, Zaib A, Ishak A, Abu Bakar S, Sherif E-SM, et al. An exact solution of a Casson fluid flow induced by dust particles with hybrid nanofluid over a stretching sheet subject to Lorentz forces. Waves Random Complex Media 2022:1−14. [CrossRef]
[39] Nadeem S, Khan MN, Abbas N. Transportation of slip effects on nanomaterial micropolar fluid flow over exponentially stretching. Alex Eng J 2020;59:3443−3450. [CrossRef]
[40] Shafiq A, Mebarek-Oudina F, Sindhu TN, Rasool G. Sensitivity analysis for Walters-B nanoliquid flow over a radiative Riga surface by RSM. Sci Iran 2022;29:1236−1249.
[41] Singh U, Gupta NK. Thermal performance analysis of heat pipe using response surface methdologyU-dayvir. J Therm Eng 2023:411−423. [CrossRef]